

A General Relativistic Calculation of Boundary Layer and Disk Luminosity for Accreting Non-magnetic Neutron Stars in Rapid Rotation

Arun V. Thampan¹ \star , and Bhaskar Datta^{1,2} \dagger

¹ *Indian Institute of Astrophysics, Bangalore 560 034, India*

² *Raman Research Institute, Bangalore 560 080, India.*

ABSTRACT

We calculate the disk and boundary layer luminosities for accreting rapidly rotating neutron stars with low magnetic fields in a fully general relativistic manner. Rotation increases the disk luminosity and decreases the boundary layer luminosity. A rapid rotation of the neutron star substantially modifies these quantities as compared to the static limit. For a neutron star rotating close to the centrifugal mass shed limit, the total luminosity has contribution only from the extended disk. For such maximal rotation rates, we find that much before the maximum stable gravitational mass configuration is reached, there exists a limiting central density, for which particles in the innermost stable orbit will be more tightly bound than those at the surface of the neutron star. We also calculate the angular velocity profiles of particles in Keplerian orbits around the rapidly rotating neutron star. The results are illustrated for a representative set of equation of state models of neutron star matter.

Key words: Stars: accretion – stars: accretion disks – stars: neutron – stars: rotation

1 INTRODUCTION

For accreting neutron stars in old binary systems, also known as low-mass X-ray binaries (LMXBs), a narrow boundary layer girdling the neutron star will form next to the neutron star surface. The importance of the boundary layer derives from the possibility that this could be the site for the emission of a variable isothermal blackbody radiation component observed in the spectra of LMXBs characterized by very high X-ray luminosity (Mitsuda et al 1984). For weak magnetic field neutron stars, the boundary layer is expected to be substantially more X-ray luminous than the entire extended accretion disk on general theoretical grounds (Sunyaev & Shakura 1986; King 1995). An important feature of disk accretion onto a weakly magnetized neutron star is that the neutron star will get spun up to its equilibrium period (\sim milliseconds), over a timescale of hundreds of millions of years (see Bhattacharya & van den Heuvel 1991 and references therein). A rapid spin of the neutron star will enhance its equatorial radius and also relocate the inner boundary of the accretion disk closer to the neutron star surface. In effect, this would imply a narrowing down of the boundary layer separation. Consequently, the boundary

layer luminosity is expected to be much smaller in comparison to the static or slowly rotating neutron star case, and this can alter the X-ray emission spectra of LMXBs.

The effect of rotation of the neutron star on the accretion luminosities was considered by Datta, Thampan & Wiita (1995), using the ‘slow’ rotation (but general relativistic) formalism due to Hartle & Thorne (1968). These authors found that rotation always increases the disk luminosity, usually decreases the boundary layer luminosity and reduces the rate of angular momentum evolution, and gave quantitative estimates corresponding to realistic neutron star models. An important parameter in this connection is the radius of the innermost stable circular orbit (r_{orb}). This quantity plays a central role in deciding the magnitude of the gravitational energy release, and hence the accretion luminosities. The relevance of r_{orb} was emphasized by Kluźniak & Wagoner (1985) who pointed out that for non-magnetic accreting neutron stars, it is incorrect to make the general assumption that the accretion disk will be separated from the neutron star surface by a thin boundary layer. The boundary layer separation will depend on whether the equation of state (EOS) of neutron star matter is stiff or soft. For rapidly rotating neutron stars, Cook, Shapiro & Teukolsky (1994) calculated the marginally stable circular orbits for application to angular momentum evolution of isolated neutron stars.

\star e-mail: arun@iiap.ernet.in

\dagger e-mail: datta@iiap.ernet.in

Accretion onto a rapidly rotating neutron star can bring in several interesting features. LMXBs are likely to accrete material whose total mass can be a substantial fraction of the neutron star mass ($\gtrsim 0.1 M_{\odot}$). This can severely reduce the magnitude of the boundary layer luminosity (King 1995). Another important question is whether or not the accreting neutron star will be disrupted once it reaches equilibrium rotation rate with further arrival of the accreted plasma. Recently, Bisnovatyi–Kogan (1993) has given a self-consistent analytical solution for an accretion disk structure around a rapidly rotating non-magnetized neutron star, using rigidly rotating polytropic model. This work also gives a simple recipe for estimating the accretion luminosities based on accreting black-hole analogy. In the present paper, we do not address the question of the disk structure or instability at equilibrium rotation rates, but examine how a rapid rotation rate of the neutron star will affect the boundary layer separation and reorder the contribution to the total accretion luminosity due to the disk and the boundary layer. The structure of rotating neutron stars in general relativity are calculated using a numerical code developed by us. This code is based on the Komatsu, Eriguchi & Hachisu (1989) formalism, as modified by Cook, Shapiro & Teukolsky (1994) to incorporate realistic neutron star equations of state. This formalism is fully general relativistic and is amenable to a self-consistent numerical treatment, employing a Newton–Raphson type iterative scheme. We find that rotation increases the disk luminosity and decreases the boundary layer luminosity, and for rotation rates near the centrifugal mass shed limit, the total luminosity has contribution only from the extended disk. Furthermore, for such maximal rotation rates, we find that much before the maximum stable gravitational mass configuration is reached, there exists a limiting central density of the neutron star for which particles in the innermost stable circular orbit will be more tightly bound than those at the surface of the rotating neutron star. We also examine the possible modifications in the angular velocity profile of the accreted material in Keplerian orbit brought on by rapid rotation of the neutron star.

The format of this paper is arranged as follows. Section 2 gives the formalism and the basic equations to be solved. Section 3 outlines the calculation of rotating neutron star models. The Keplerian angular velocity profiles are described in section 4. The results of our calculations are summarized in section 5 and a discussion given in section 6.

2 ACCRETION LUMINOSITIES FOR A ROTATING SPACE–TIME

The space–time around a rotating neutron star can be described in quasi–isotropic coordinates, as a generalization of Bardeen’s metric (Bardeen 1970):

$$ds^2 = -e^{\gamma+\rho} dt^2 + e^{2\alpha} (dr^2 + r^2 d\theta^2) + e^{\gamma-\rho} r^2 \sin^2 \theta (d\phi - \omega dt)^2 \quad (1)$$

where the metric potentials γ , ρ , α , and the angular velocity of the stellar fluid relative to the local inertial frame (ω) are all functions of the quasi–isotropic radial coordinate (r) and the polar angle (θ). We use here geometric units: $c = 1 = G$.

Since the metric is stationary and axisymmetric, the energy and angular momentum are constants of motion. Therefore, the specific energy \tilde{E} (in units of the rest energy $m_0 c^2$, where m_0 is the rest mass of the accreted particle) and the specific angular momentum l (in units of $m_0 c$) can be identified as $-p_0$ and p_3 respectively, where, p_{μ} ($\mu = 0, 1, 2, 3$), stands for the four-momentum of the particle. From the condition $p_{\mu} p^{\mu} = -1$, we have the equations of motion of the particle (confined to the equatorial plane) in this gravitational field as

$$\dot{t} = \frac{dt}{d\tau} = p^0 = e^{-(\gamma+\rho)} (\tilde{E} - \omega l) \quad (2)$$

$$\dot{\phi} = \frac{d\phi}{d\tau} = p^3 = \Omega p^0 = e^{-(\gamma+\rho)} \omega (\tilde{E} - \omega l) + \frac{l}{r^2 e^{(\gamma-\rho)}} \quad (3)$$

$$\dot{r}^2 \equiv e^{2\alpha+\gamma+\rho} \left(\frac{dr}{d\tau} \right)^2 = \tilde{E}^2 - \tilde{V}^2. \quad (4)$$

Here Ω is the angular velocity of the star as seen by a distant observer, $d\tau$ is the proper time and \tilde{V} is the effective potential given by

$$\tilde{V}^2 = e^{\gamma+\rho} \left[1 + \frac{l^2/r^2}{e^{\gamma-\rho}} \right] + 2\omega \tilde{E} l - \omega^2 l^2. \quad (5)$$

The conditions for circular orbits, extremum of energy and minimum of energy are respectively:

$$\tilde{E}^2 = \tilde{V}^2 \quad (6)$$

$$\tilde{V}_{,r} = 0 \quad (7)$$

$$\tilde{V}_{,rr} > 0. \quad (8)$$

For marginally stable orbits,

$$\tilde{V}_{,rrr} = 0. \quad (9)$$

In our notation, a comma followed by one ‘ r ’ represents a first order partial derivative with respect to r and so on, and a tilde over a variable represents the corresponding dimensionless quantity.

From the expression for the effective potential and the conditions (6), (7) and (9), one obtains three equations in three unknowns, namely, r , \tilde{E} , and l . In principle, if analytical expressions for $e^{\gamma+\rho}$, $e^{2\alpha}$, $e^{\gamma-\rho}$ and ω are known, it would be a straightforward exercise to solve these equations to obtain r , \tilde{E} , and l . In practice, however, this is not so, and the solutions for the metric coefficients $e^{\gamma+\rho}$, $e^{2\alpha}$, $e^{\gamma-\rho}$, and ω have to be obtained as arrays of numbers for various values of r and θ using a numerical treatment. Furthermore, the condition (9) will introduce second order derivatives of γ , ρ , and ω , which means that care has to be exercised in ensuring the numerical accuracies of the quantities calculated. For this purpose, it is convenient to express \tilde{E} and l in terms of the physical velocity \tilde{v}

$$\tilde{v} = (\Omega - \omega) r e^{-\rho} \sin \theta \quad (10)$$

of the stellar matter with respect to a locally nonrotating observer (see Bardeen 1972).

This gives the following expressions:

$$\tilde{E} - \omega l = \frac{e^{(\gamma+\rho)/2}}{\sqrt{1-\tilde{v}^2}} \quad (11)$$

$$l = \frac{\tilde{v} r e^{(\gamma-\rho)/2}}{\sqrt{1-\tilde{v}^2}}. \quad (12)$$

Equations (11) and (12) can be recognized as the condition for circular orbits. Conditions (7) and (9) yield respectively,

$$\tilde{v} = \frac{e^{-\rho} r^2 \omega_{,r} \pm [e^{-2\rho} r^4 \omega_{,r}^2 + 2r(\gamma_{,r} + \rho_{,r}) + r^2(\gamma_{,r}^2 - \rho_{,r}^2)]^{1/2}}{2 + r(\gamma_{,r} - \rho_{,r})} \quad (13)$$

$$\begin{aligned} \tilde{V}_{,rr} \equiv & 2 \left[\frac{r}{4} (\rho_{,r}^2 - \gamma_{,r}^2) - \frac{1}{2} e^{-2\rho} \omega_{,r}^2 r^3 - \rho_{,r} + \frac{1}{r} \right] \tilde{v}^2 \\ & + [2 + r(\gamma_{,r} - \rho_{,r})] \tilde{v} \tilde{v}_{,r} - e^{-\rho} \omega_{,r} r \tilde{v} \\ & + \frac{r}{2} (\gamma_{,r}^2 - \rho_{,r}^2) - e^{-\rho} r^2 \omega_{,r} \tilde{v}_{,r} = 0 \end{aligned} \quad (14)$$

where we have made use of Eq. (13) and its derivative with respect to r in order to eliminate the second order derivatives in Eq. (14). The zero of $\tilde{V}_{,rr}$ will give the innermost stable circular orbit radius (r_{orb}) and the corresponding \tilde{v} will yield \tilde{E} and l . In equation (13), the positive sign refers to the co-rotating particles and the negative sign to the counter-rotating particles. In this study we have considered only the co-rotation case.

Depending on the EOS and the central density, neutron stars can have radii greater than or less than r_{orb} (Datta, Thampan & Wiita 1995). The accretion luminosities will, of course, be different for these two cases (Kluźniak and Wagoner 1985; Sunyaev and Shakura 1986; Datta, Thampan and Wiita 1995). These quantities can be calculated as follows: Case (a): Radius of the star (R) greater than r_{orb} .

If an accretion disk were to form around a relatively large neutron star, the ingress of a particle of rest mass m_0 from infinity to the disk boundary (which will be at the stellar surface) will release an amount of energy given by:

$$E_D = m_0 \{1 - \tilde{E}_K(r=R)\} \quad (15)$$

where $\tilde{E}_K(r=R)$ is the specific energy of the particle in Keplerian orbit at the surface obtained by solving equation (13) to obtain $\tilde{v}_K = \tilde{v}$ and solving equations (11) and (12) with $r=R$ and $\tilde{v} = \tilde{v}_K$ to obtain l_K and $\tilde{E}_K(r=R)$.

The energy loss in the boundary layer (a very narrow gap near the neutron star surface) will be

$$E_{BL} = m_0 \{ \tilde{E}_K(r=R) - \tilde{E}_0 \} \quad (16)$$

where \tilde{E}_0 is the energy of the particle ‘‘at rest’’ on the stellar surface (the particle will be moving with the velocity $\tilde{v} = \tilde{v}_*$ of the stellar fluid at the surface, where \tilde{v}_* is obtained by substituting into equation (10) all the relevant parameters for $r=R$) and is calculated by solving equations (11) and (12) for \tilde{E} at $r=R$ and $\tilde{v} = \tilde{v}_*$.

Case (b): Radius of the star (R) smaller than radius of r_{orb} .

In this case, the accretion disk will extend inward to a radius corresponding to $r = r_{orb}$. The energy released in the disk as the particle comes in from infinity to the innermost stable circular orbit will be

$$E_D = m_0 \{1 - \tilde{E}_{orb}\}. \quad (17)$$

The energy released in the boundary layer will be

$$E_{BL} = m_0 \{ \tilde{E}_{orb} - \tilde{E}_0 \} \quad (18)$$

where \tilde{E}_{orb} is the energy of the particle in innermost stable circular orbit, calculated by finding the $r = r_{orb}$ at which equation (14) is satisfied and then solving equations (11), (12) and (13) for this r to yield \tilde{E}_{orb} . The energy \tilde{E}_0 of the particle on the stellar surface is calculated as described in the previous case.

3 ANGULAR VELOCITY PROFILES

For slow rotation of the neutron star, the angular velocity of the accreted material in Keplerian orbit around it, $\Omega(r)$, will have a profile that has a maximum that is located outside the neutron star surface. For rapid rotation rates of the star (corresponding to angular velocity close to the Keplerian value at the surface), a second type of profile for $\Omega(r)$ is also possible, in which $\Omega(r)$ exhibits no maximum but increases monotonically all the way to the surface of the neutron star. In such a situation, the accretion torque on the neutron star will not be purely advective. It will become possible for the viscous torque to transport angular momentum outwards at all radii. This can lead to interesting accretion scenarios.

The Keplerian angular velocity Ω_K of a particle in an orbit around the rotating neutron star is defined as:

$$\Omega_K(r) = e^{\rho(r)} \frac{\tilde{v}(r)}{r} + \omega(r) \quad (19)$$

where \tilde{v} is as given in equation (12). The Keplerian angular velocity of the particle in an orbit at the surface of the neutron star puts a firm upper bound on the angular velocity the star can attain (Friedman, Ipser and Parker 1986) and hence the boundary layer luminosity when the star attains this maximum Ω should be zero (Sunyaev and Shakura 1986).

4 RAPIDLY ROTATING NEUTRON STAR MODELS IN GENERAL RELATIVITY

Rapidly rotating neutron star structure in general relativity for realistic neutron star EOS have been reported by Friedman, Ipser & Parker (1986). Their numerical code is based on the programmes developed by Butterworth & Ipser (1976). Previous models of rapidly rotating neutron stars have been based on incompressible fluids and polytropic models (Bonazzola & Schneider 1974; Butterworth 1976). Komatsu, Eriguchi & Hachisu (1989) have generalized the Newtonian self-consistent field method to a general relativistic case to obtain structures of rapidly rotating stars, again using the polytropic model. This technique was modified by Cook, Shapiro & Teukolsky (1994) for realistic neutron star EOS for purpose of studying quasi-stationary evolution of isolated neutron stars. A variant of this approach based on spectral methods was developed by Bonazzola et al. (1993).

In this investigation, we have calculated the structure of rapidly rotating neutron stars in general relativity using a numerical code developed by the present authors, which is based on the method due to Komatsu, Eriguchi & Hachisu (1989), as modified by Cook, Shapiro & Teukolsky (1994) so as to incorporate realistic neutron star EOS. The results of our code agree with the published results of Friedman, Ipser & Parker (1986), and results using the code of Stergioulas & Friedman (1995) to less than 1%. Also, wherever a comparison was possible, our results agreed with those reported in Cook, Shapiro & Teukolsky (1994) to a similar degree of accuracy. For non-rotating equilibrium models, we found our results to be within 0.3% of the published results of Arnett and Bowers (1977). We have constructed numerically various sequences of neutron stars, starting from the static limit all the way upto the rotation rate corresponding to the centrifugal mass shed limit. The latter limit corresponds to the maximum Ω for which centrifugal forces are able to balance the inward gravitational force. Any further increase in Ω will lead to disruption of the star. The general relativistic expression for this limit can be found in Cook, Shapiro & Teukolsky (1994).

The structure of neutron stars depends sensitively on the EOS at high densities. Although the main composition of degenerate matter at densities higher than nuclear matter density is expected to be dominated by neutrons, significant admixtures of other elementary particles (such as pions, kaons and hyperons) are not ruled out. A persistent problem in determining the EOS for neutron star interior is what to choose for the interaction potential among the constituent particles, for which reliable experimental data are not available. All calculations involve either extrapolations from known nuclear matter properties or plausible field theoretical approaches using mean field approximation. Another related but unresolved problem is: what is an adequate many-body technique to estimate the higher order correlation terms in expressions for the pressure. In this paper we do not address these problems, but choose, for illustrating the results of the present study, six EOS models based on representative neutron star matter interaction models. This is expected to provide a broad realistic set of conclusions. A brief description of the EOS models used here is given below.

(A) *Pandharipande (1971) (hyperonic matter)*: One of the early attempts to derive nuclear EOS with admixture of hyperons is due to Pandharipande (1971), who assumed the hyperonic potentials to be similar to the nucleon-nucleon potentials, but altered suitably to represent the different isospin states. The many-body method adopted is based on the variational approach of Jastrow (1955). The two body wave function was taken as satisfying a simplified form of the Bethe-Goldstone equation, in which terms representing the Pauli exclusion principle were omitted but simulated by imposing a ‘healing’ constraint on the wave function.

(B) *Bethe-Johnson*: Bethe & Johnson (1974) devised phenomenological potentials for nucleon-nucleon interaction that have realistic short-range behaviour. These authors then used the lowest order constrained variational method to calculate the EOS of neutron star matter. The work of Bethe & Johnson (1974) consists of two different parts: (a) determination of the EOS for pure neutron gas and (b) derivation

of a hyperonic equation of state. For purpose of illustration here, we have chosen their EOS model V (neutron matter).

(C) *Walecka (1974) (neutrons)*: The EOS model of Walecka (1974) corresponds to pure neutron matter, and is based on a mean-field theory with exchange of scalar and (isoscalar) vector mesons representing the nuclear interaction.

(D) *Wiringa, Fiks & Fabrocini (1988) (UV14 + UVII)*: These authors gave a model of EOS for dense nuclear and neutron matter which includes three-nucleon interactions. This is a non-relativistic approach based on the variational method. The three-body potential includes long-range repulsive parts that are adjusted to give light nuclei binding energies and nuclear matter saturation properties. The authors have given three models. We consider here their model UV14+UVII for beta-stable case: neutrons, protons, electrons and muons.

(E) *Sahu, Basu & Datta (1993)*: gave a field theoretical EOS for neutron-rich matter in beta equilibrium based on the chiral sigma model. The model includes an isoscalar vector field generated dynamically and reproduces the empirical values of the nuclear matter saturation density and binding energy and also the isospin symmetry coefficient for asymmetric nuclear matter. The energy per nucleon of nuclear matter according to Sahu, Basu & Datta (1993) is in very good agreement, up to about four times the equilibrium nuclear matter density, with estimates inferred from heavy-ion collision experimental data.

(F) *Baldo, Bombaci & Burgio (1997)*: have recently given a microscopic EOS for asymmetric nuclear matter, derived from the Brueckner-Bethe-Goldstone many-body theory with explicit three-body terms. The three-body force parameters are adjusted to give a reasonable saturation point for nuclear matter.

The pressure-density relationship of these above EOS models is illustrated in Fig 1. Of the above EOS, model (A) is a relatively soft EOS, models (B), (D) and (F) are roughly intermediate in stiffness, whereas models (C) and (E) are rather stiff EOS. It may be recalled that a stiffer EOS will give a higher value for the non-rotating neutron star maximum mass and also a higher value for the corresponding radius. The composite EOS for the entire span of neutron star densities was constructed by joining the selected high density EOS to that of Negele & Vautherin (1973) for the density range ($10^{14} - 5 \times 10^{10}$) $g\ cm^{-3}$, Baym, Pethick & Sutherland (1971) for densities down to $\sim 10^3\ g\ cm^{-3}$ and Feynman, Metropolis & Teller (1949) for densities less than $10^3\ g\ cm^{-3}$.

We found that while the results for EOS’s (B), (C), (E) and (F) were straightforward, EOS models (A) and (D) presented the peculiarity of having the maximum Ω model as the maximum stable mass model (in agreement with the result of Cook, Shapiro & Teukolsky 1994) suggesting that EOS’s (A) and (D) belong to the Class I EOS and EOS models (B), (C), (E) and (F) to Class II as classified in Stergioulas & Friedman (1995).

5 RESULTS

All the calculated parameters depend on the central density (ρ_c) and rotation rate (Ω) of the neutron star. In Table 1 we

Table 1. The values of the neutron star gravitational mass M_G , disk luminosity E_D , boundary layer luminosity E_{BL} , the boundary layer separation (i.e, the height above stellar surface, where the innermost stable circular orbit is located) h^+ and the Keplerian angular velocity Ω_K for two values of neutron star rotation rates $\Omega = 0$ and $\Omega = \Omega_{ms}$ and chosen values of central density ρ_c – see text for details. The numbers following the letter E in column 9 stand for powers of ten. ρ_c is in units of $10^{14} \text{ g cm}^{-3}$; Ω_{ms} and Ω_K are in units of 10^4 rad s^{-1} .

EOS	ρ_c	Ω_{ms}	M		E_D		E_{BL}		h^+		Ω_K	
			(M_\odot)		$(m_\odot c^2)$		$(m_\odot c^2)$		(km)		$\Omega = 0$	$\Omega = \Omega_{ms}$
			$\Omega = 0$	$\Omega = \Omega_{ms}$	$\Omega = 0$	$\Omega = \Omega_{ms}$	$\Omega = 0$	$\Omega = \Omega_{ms}$	$\Omega = 0$	$\Omega = \Omega_{ms}$	$\Omega = 0$	$\Omega = \Omega_{ms}$
(A)	26.630	1.105	1.183	1.400	0.057	0.073	0.177	$1.578E-4$	2.052	0.000	1.167	1.106
	*39.121	1.370	1.357	1.585	0.057	0.084	0.246	$1.141E-4$	4.239	0.000	1.018	1.370
	43.000	1.434	1.381	1.608	0.057	0.085	0.261	$-9.000E-6$	4.616	0.223	1.000	1.387
(B)	10.670	0.718	1.133	1.400	0.056	0.058	0.110	$4.970E-5$	—	—	1.065	0.718
	13.730	0.847	1.400	1.723	0.057	0.071	0.160	$6.780E-5$	1.719	0.000	0.986	0.847
	*22.600	1.062	1.694	2.034	0.057	0.084	0.237	$1.866E-4$	5.057	0.000	0.815	1.063
	26.000	1.119	1.730	2.060	0.057	0.086	0.254	$1.160E-5$	5.619	0.286	0.798	1.082
	35.270	1.240	1.757	2.060	0.057	0.088	0.284	$-9.098E-4$	6.403	0.721	0.786	1.133
(C)	6.363	0.609	1.088	1.400	0.053	0.053	0.090	$3.880E-5$	—	—	0.900	0.609
	7.413	0.689	1.400	1.818	0.057	0.065	0.128	$1.058E-4$	0.137	—	0.985	0.689
	*10.610	0.845	1.961	2.493	0.057	0.084	0.217	$2.199E-4$	5.140	0.000	0.704	0.845
	19.500	1.042	2.279	2.769	0.057	0.094	0.303	$-3.196E-3$	8.799	1.408	0.606	0.905
	21.750	1.070	2.284	2.757	0.057	0.094	0.311	$-3.877E-3$	9.020	1.508	0.605	0.918
(D)	8.757	0.700	1.106	1.400	0.056	0.057	0.104	$5.593E-5$	—	—	1.033	0.700
	10.430	0.803	1.400	1.780	0.057	0.070	0.150	$7.670E-5$	1.297	0.000	0.986	0.803
	*13.530	0.953	1.788	2.239	0.057	0.084	0.223	$1.055E-4$	4.896	0.000	0.772	0.954
	22.270	1.217	2.160	2.604	0.057	0.097	0.331	$-6.517E-3$	8.946	1.640	0.640	1.013
(E)	3.556	0.465	1.059	1.400	0.047	0.047	0.069	$1.412E-4$	—	—	0.692	0.466
	4.064	0.520	1.400	1.887	0.055	0.057	0.097	$7.938E-5$	—	—	0.761	0.520
	*6.996	0.674	2.338	3.043	0.057	0.083	0.207	$1.836E-4$	5.641	0.000	0.591	0.674
	11.000	0.762	2.572	3.221	0.057	0.089	0.254	$-4.476E-4$	8.341	0.865	0.537	0.711
	13.394	0.794	2.589	3.200	0.057	0.089	0.266	$-8.943E-4$	8.841	1.038	0.534	0.730
(F)	9.136	0.697	1.106	1.400	0.056	0.057	0.104	$1.149E-4$	—	—	1.030	0.697
	11.900	0.812	1.398	1.760	0.057	0.070	0.152	$1.012E-4$	1.382	0.000	0.988	0.812
	*20.493	1.019	1.732	2.109	0.057	0.084	0.233	$9.228E-5$	5.031	0.000	0.797	1.019
	26.000	1.100	1.780	2.135	0.057	0.086	0.257	$-1.487E-4$	5.837	0.380	0.776	1.053
	30.890	1.155	1.788	2.126	0.057	0.087	0.270	$-5.163E-4$	6.199	0.568	0.772	1.080

have summarized the functional dependences on ρ_c of some important parameters in the calculation of luminosities. In order to illustrate this dependence, we choose two limits of Ω , namely, the non-rotating or static limit ($\Omega = 0$) and the centrifugal mass shed limit ($\Omega = \Omega_{ms}$), which are the two natural ends of a constant density sequence. As expected, the functional form of the dependence of structure parameters on central density for rotation rate at centrifugal mass shed limit ($\Omega = \Omega_{ms}$) is found to be qualitatively similar to that at the static limit and so are not explicitly displayed here (see, for example Friedman, Ipser & Parker 1986). The listed quantities in Table 1 are the values of the neutron star gravitational mass M_G , disk luminosity E_D , boundary layer luminosity E_{BL} , the boundary layer separation (i.e, the height above stellar surface, where the innermost stable circular orbit is located) h^+ and the Keplerian angular velocity Ω_K . Generally speaking, r_{orb} exhibits three char-

acteristics: (a) r_{orb} is non-existent, (b) $r_{orb} < R$, and (c) $r_{orb} > R$. For the first two cases, the r_{orb} is taken to be the Keplerian orbit radius at the surface of the star. The cases for which r_{orb} is non-existent are differentiated in Table 1 by a dashed line under the column for h^+ and the cases for which $r_{orb} \leq R$ are indicated by the entries for which h^+ is zero. The central density at which r_{orb} exactly equals R in the rotating case (we call this the radius cross-over density), is indicated by an asterisk over the corresponding central density. For each EOS model, we choose five central densities corresponding to: (i) $M_G = 1.4 M_\odot$ at $\Omega = \Omega_{ms}$, (ii) $M_G = 1.4 M_\odot$ at $\Omega = 0$, (iii) the radius cross-over density, at which $r_{orb} = R$ for $\Omega = \Omega_{ms}$, (iv) $M_G = \text{maximum mass}$ at $\Omega = \Omega_{ms}$ and (v) $M_G = \text{maximum mass}$ at $\Omega = 0$. For neutron stars corresponding to the EOS models (A) and (D), we find that before the maximum stable mass is attained, the sequences become unstable to radial perturbations, and

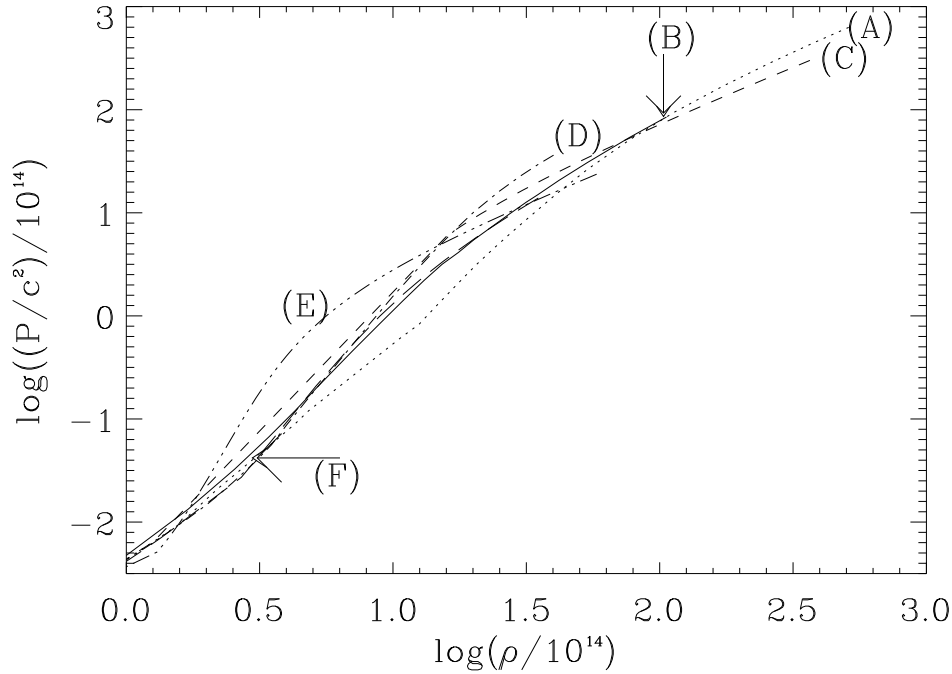


Figure 1. Pressure as a function of density for the EOS models (A–F).

hence the corresponding maximum Ω model can be taken as the maximum mass stable model. Therefore, in Table 1 we have listed, for these EOS, parameters corresponding to the maximum Ω model instead of the maximum mass model.

From Table 1, it can be seen that typical increases in mass (to maintain the central density constant) from the static limit is (14–35)%, with the larger changes corresponding to the lower densities in the stiffer EOS. The corresponding increase in radius (see Fig. 4) lie in the range (28–44)%.

Table 1 also shows that the disk luminosity E_D increases for $\Omega = \Omega_{ms}$ with central density whereas, in the non-rotating case, it remains constant (except in the low central density regime for the stiff EOS for which the r_{orb} is located at the surface of the star). On the other hand, E_{BL} is substantially higher (almost by a factor of 2) than E_D in the static limit but becomes almost zero at the centrifugal mass shed limit (because of the fact that rotation rate at this limit is very nearly equal to the Kepler frequency of a particle in the innermost stable circular orbit at the surface). Interestingly, E_{BL} is negative for densities higher than the radius cross-over density.

In Fig. 2, we display the dependence of Ω_{ms} with ρ_c . Ω_{ms} varies monotonically with ρ_c . Furthermore, Ω_{ms} seems to possess a marked dependence on the EOS; the softer the EOS, the larger the value of Ω_{ms} . All curve labels in Figs 2, 3, 5 and 7 are as indicated in Fig 1.

The variation of the gravitational mass M_G , baryonic mass M_0 , stellar radius R , and the radius r_{orb} of the innermost stable circular orbit with respect to Ω for the radius cross-over density is illustrated in Fig. 3. From Fig 3, it can be seen that until $\Omega \sim 0.5\Omega_{ms}$, the structure parameters change slowly but for higher rotation rates ($\Omega \gtrsim 0.6\Omega_{ms}$), the rate

of change is more pronounced. These changes are EOS dependent, being more substantial for stiffer EOS.

To illustrate how the boundary layer separation varies with ρ_c , Ω and also with the EOS, we give in Fig. 4, plots of r_{orb} and R versus ρ_c for two cases of Ω . In Fig. 4, the six graphs corresponding to the different EOS models, display $R(\Omega = 0)$ (curve 1), $R(\Omega = \Omega_{ms})$ (curve 2), $r_{orb}(\Omega = 0)$ (curve 3) and $r_{orb}(\Omega = \Omega_{ms})$ (curve 4). It is immediately apparent from the plots that as Ω increases from 0 to Ω_{ms} for a fixed ρ_c , R (curves 1 and 2) increases and r_{orb} (curves 3 and 4) decreases. Furthermore, it can be seen that in the static case r_{orb} is generally greater than R for the whole range of central densities, the exception being for the stiff EOS (C) and (E) (in these latter cases, r_{orb} is less than R for a few lower central density values), whereas at the centrifugal mass shed limit, r_{orb} is greater than R only for very high densities. The intersection of curve (2) with curve (4) represents the cross-over density ρ_c for which $r_{orb} = R$ at the centrifugal mass shed limit. Since at the mass shed limit, the stellar rotation rate is almost equal to the angular velocity of a particle in Keplerian orbit at the surface of the star, the radius cross-over density represents the point at which the particle in the innermost stable circular orbit will start becoming more bound than a particle at the surface of the star. In other words, E_{BL} will tend to zero at this central density and will become negative at some central density greater than this. This is indicated by the vertical line in the graph.

In Fig. 5, we plot E_D , E_{BL} , the total luminosity ($E_D + E_{BL}$) and the ratio of E_{BL} to E_D , all as functions of Ω/Ω_{ms} . All these plots are for radius cross-over density for the various EOS. Among the various EOS, E_D differs

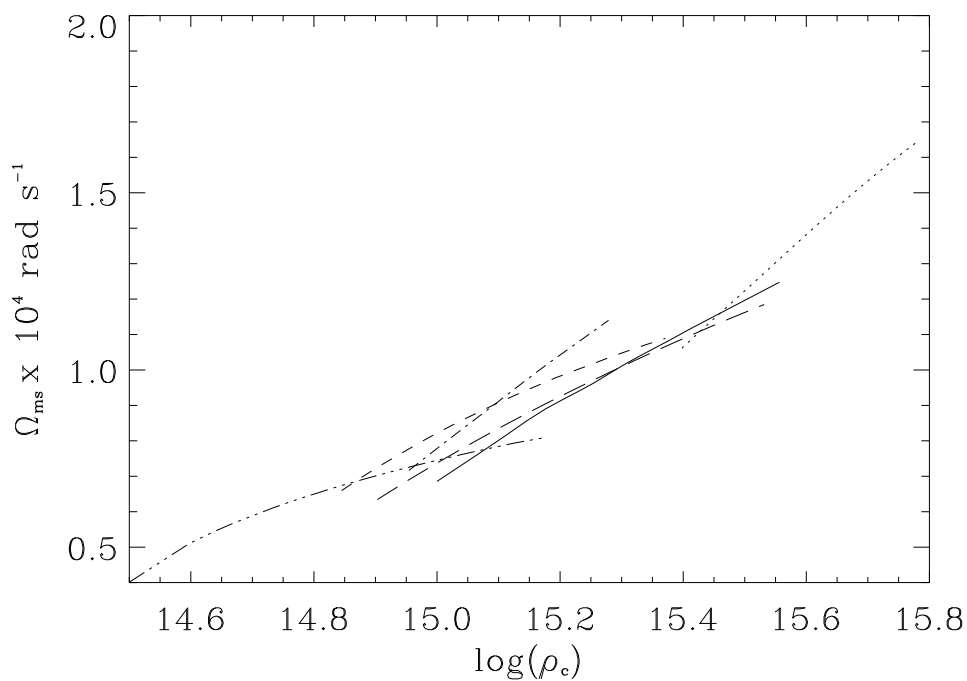


Figure 2. The neutron star rotation rate at the centrifugal mass shed limit as a function of central density for various EOS models. The labels in Figs 2, 3, 5 & 7 are as in Fig 1.

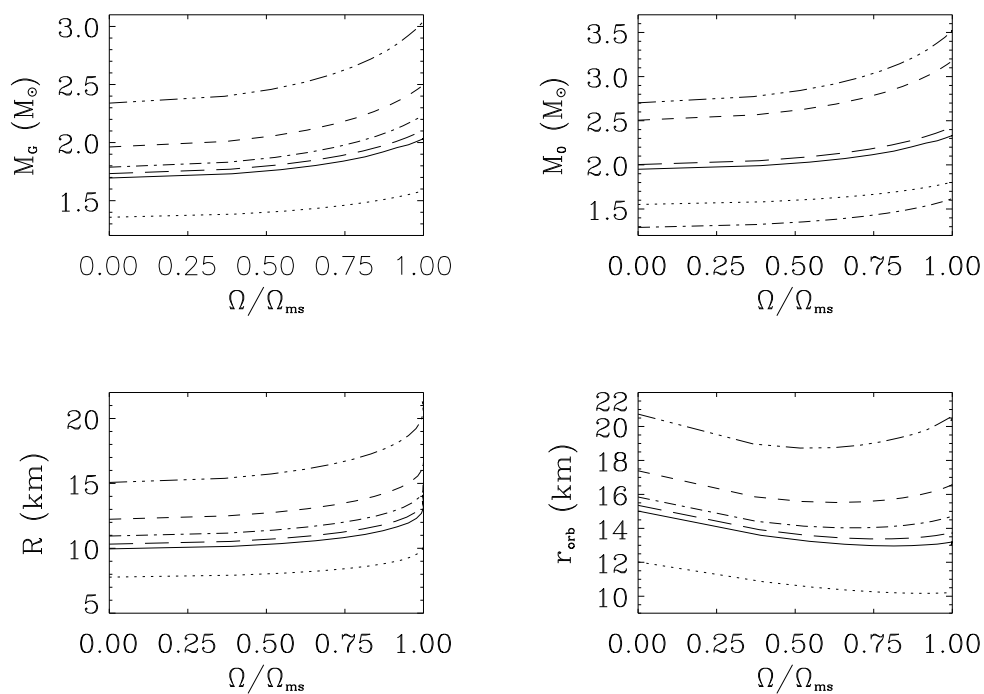


Figure 3. Neutron star gravitational mass (M_G), baryonic mass (M_0), radius (R), and the radius (r_{orb}) of the innermost stable circular orbit as a function of the star's rotation rate for various EOS. The graphs correspond to the radius cross over central density for each EOS.

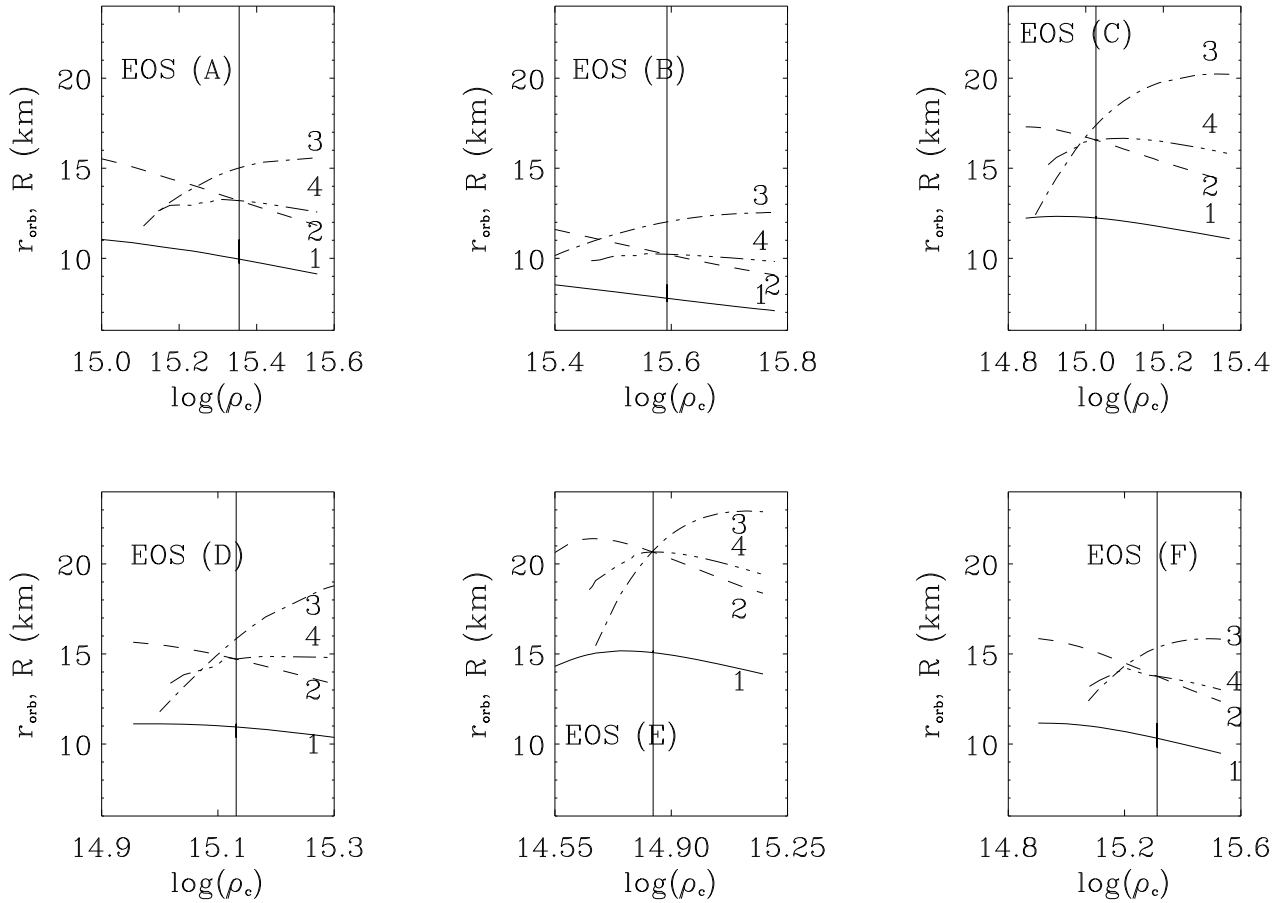


Figure 4. Neutron star radius (R) and radius (r_{orb}) of the innermost stable circular orbit as functions of central density for two values of stellar rotation rate (Ω). See text for the details.

most when Ω is large. In contrast, E_{BL} differs (among the various EOS), most for slow rotation rates. Therefore, the total luminosity follows a variation similar to that of E_{BL} .

The dependence of Ω_K on Ω is shown in Fig 6. For convenience of display and comparison, these are taken in units of Ω_{ms} , and two chosen values of ρ_c . In Fig 6 curve 1 refers to ρ_c corresponding to $M_G = 1.4 M_\odot$ at static limit and curve 2 refers to ρ_c for the radius cross-over density. The qualitative differences in the behaviour of curve 1 for all the graphs is quite noticeable. These differences arise entirely due to the differences in the location of the innermost stable circular orbit with respect to the stellar surface.

In Fig. 7 we give plots of the angular velocity profiles for the radius cross over densities for each of the EOS.

6 DISCUSSIONS

In this paper we have investigated in a general relativistic manner, the effect of rapid rotation on the boundary layer and disk luminosity for an accreting, old neutron star. The

assumption made is that the magnetic field of the neutron star is too small to affect the accretion flow. It is relevant to ask if a quantitative estimate is possible of how low the magnetic field should be for the validity of our calculations. The Alfvén radius (r_A) is defined by the relationship (see Lamb, Pethick & Pines 1973)

$$\frac{B^2(r_A)}{8\pi} = \rho(r_A)v^2(r_A) \quad (20)$$

where ρ and v are respectively the density and radial velocity in the accretion disk. The Alfvén radius determines the location at which magnetic pressure channels the flow from a disk into an accretion column structure above the magnetic poles. Lamb, Pethick & Pines (1973) show that

$$r_A \lesssim 2.6 \times 10^8 \left[\frac{\mu_{30}^{4/7} (M/M_\odot)^{1/7}}{L_{37}^{2/7} R_6^{2/7}} \right] \text{cm} \quad (21)$$

where $\mu_{30} = B_0 R^3 / 10^{30} \text{ G cm}^3$, L_{37} is the total luminosity in units of $10^{37} \text{ ergs s}^{-1}$, $R_6 = R/10^6 \text{ cm}$ and B_0 is the

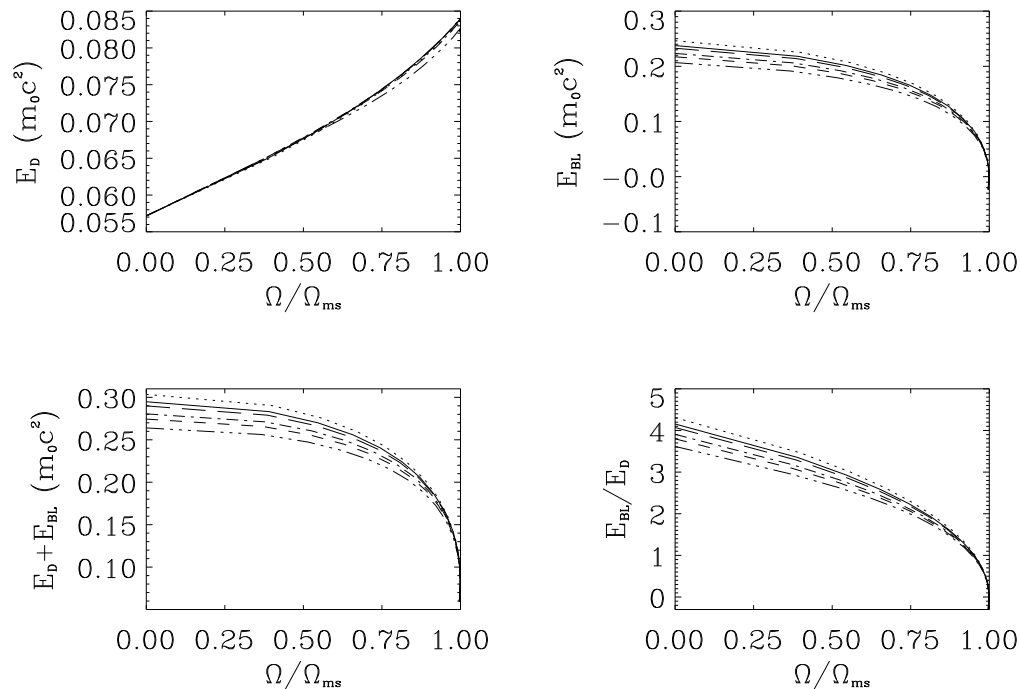


Figure 5. The accretion luminosities in units of the rest mass of the accreted particle as functions of neutron star rotation rate. The graphs correspond to the radius cross-over central density for each EOS.

magnetic field on the surface of the neutron star in gauss. The condition that $r_A < R$ implies that (for the reasonable choice: $M = 1.4 M_\odot$ and $R_6 = 1$):

$$B_0 < 5.5 \times 10^7 L_{37}^{1/2} \quad (22)$$

and is necessary for the scenario we have considered to be fully self-consistent. In our notation, $L = (E_D + E_{BL})\dot{M}c^2$, with \dot{M} the mass accretion rate.

The main conclusions of this paper are that rotational effects of general relativity increase the disk luminosity and more importantly from the point of observations, decrease the boundary layer luminosity. These effects are small in magnitude for small values of Ω but become substantial for rapid rotation rates of the neutron star. The boundary layer luminosity becomes inconsequential for rotation rates near the centrifugal mass shed limit. For such cases, the role of radiation pressure on the accretion flow (see Miller & Lamb 1996) must be re-examined. Also for such cases, accretion induced changes in the surface properties of the neutron star is an important question to investigate. The vanishing of the boundary layer luminosity for rapid rotation rates as found in this study is not apparent in a similar calculation using the “slow” rotation approximation based on the Hartle & Thorne (1968) metric (see Datta, Thampan & Wiita 1995). The total luminosity remains fairly constant upto rotation rate of about $0.6\Omega_{ms}$, but declines rapidly to the value of the disk luminosity for higher rotation rates. We have not considered here the angular momentum evolution of the accreting neutron star, but have calculated the accretion luminosities for chosen fixed values of Ω . So, the boundary layer

luminosity values listed in Table 1 do not include corrections for the energy that may go into the spinning up of the neutron star. We have not considered the effect of viscosity on the accretion luminosity. The viscosity effects require a full hydrodynamic treatment and also the radiative transfer phenomenon.

An interesting conclusion of the present study (see Fig 4) is that neutron star configurations with high central densities have their innermost stable circular orbit located exterior to the star. For such configurations that are rotating at the centrifugal mass shed limit, particles in the innermost stable circular orbit are more bound than particles at the surface of the star. This could lead to the formation of an inner disk torus. The idea of an inner disk torus has been invoked as a possible explanation of flaring branch phenomena observed in certain Quasi Periodic Oscillators (Kuulkers & van der Klis 1995), with radiation pressure playing an key dynamical role. Our study seems to suggest that an inner disk torus can be formed in the absence of a substantial radiation pressure, purely as a consequence of general relativistic rotational space-time in situations where the rotation rate of the accreting neutron star is close to the centrifugal mass shed limit.

ACKNOWLEDGEMENTS

We thank J. Friedman and N. Stergioulas for supplying us with their code for rapidly rotating neutron stars, which helped in checking the accuracy of our code. Thanks are also due to I. Bombaci for the Baldo-Bombaci-Burgio EOS tables and G. Srinivasan and R. Nayak for helpful comments.

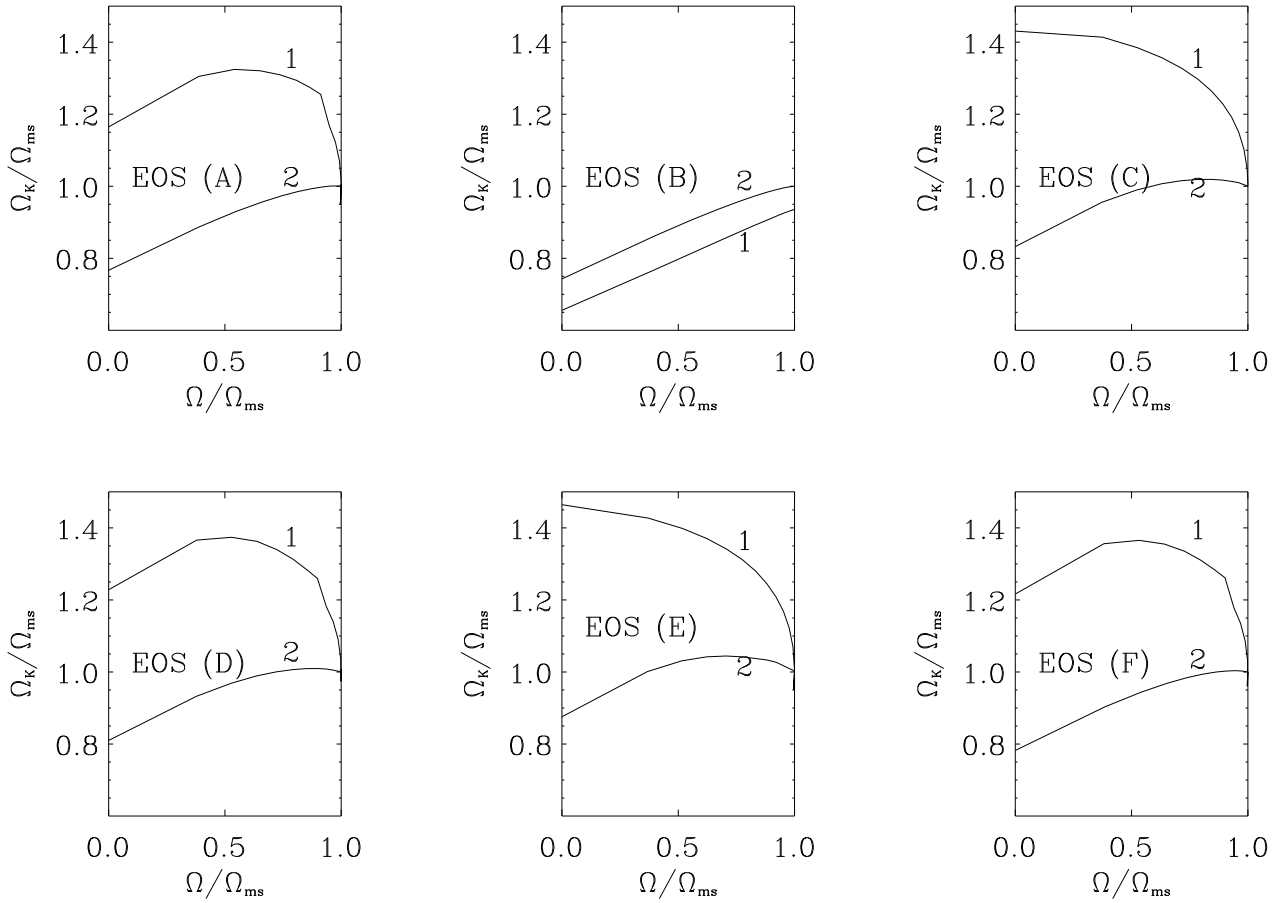


Figure 6. The Keplerian angular velocity of a particle in the innermost stable circular orbit as a function of the neutron star rotation rate. Curve 1 refers to the central density corresponding to a gravitational mass of $1.4 M_{\odot}$ in the static limit, and curve 2 corresponds to that at the radius cross-over central density.

REFERENCES

- Arnett W. D., Bowers, R. L., 1977, *ApJS*, 33, 415
 Baldo M., Bombaci I., Burgio G. F., 1997, *A&A* in press
 Bardeen J. M., 1970, *ApJ*, 162, 71
 Bardeen J. M., 1972, *ApJ*, 178, 347
 Baym G., Pethick C. J., Sutherland P. G., 1972, *ApJ*, 170, 299
 Bethe H. A., Johnson M. B., 1974, *Nucl. Phys.*, A230, 1
 Bhattacharya D., van den Heuvel E. P. J., 1991, *Phys. Repts.*, 203, 1
 Bisnovatyi-Kogan G. S., 1993, *A&A*, 274, 796
 Bonazzola S., Schneider J., 1974, *ApJ*, 191, 273
 Butterworth E. M., 1976, *ApJ*, 204, 561
 Butterworth E. M., Iper J. R., 1976, *ApJ*, 204, 200
 Cook G.B., Shapiro S.L., Teukolsky S.A., 1994, *ApJ*, 424, 823
 Datta B., Thampan A. V., Wiita P. J., 1995, *JA&A*, 16, 357
 Friedman J. L., Iper J. R., Parker L., 1986, *ApJ*, 304, 115
 Feynman R. P., Metropolis N., Teller E., 1949, *Phys. Rev.*, 75, 1561
 Hartle J. B., Thorne K. S., 1968, *ApJ*, 153, 807
 Jastrow R., 1955, *Phys. Rev.*, 98, 1479
 King A., 1995, in Lewin W. H. G., van Paradijs J., van den Heuvel E. P. J., eds., *X-Ray Binaries*. Cambridge Univ. Press, p. 419
 Kluźniak W., Wagoner R. V., 1985, *ApJ*, 297, 548
 Komatsu H., Eriguchi Y., Hachisu I., 1989, *MNRAS*, 237, 355
 Kuulkers E., van der Klis M., 1995, *A&A*, 303, 801
 Lamb F.K., Pethick C. J., Pines D., 1973, *ApJ*, 184, 279
 Miller M. C., Lamb F. K., 1996, *ApJ*, 470, 1033
 Mitsuda K. et al, 1984, *PASJ*, 36, 741
 Negele J. W., Vautherin D., 1973, *Nucl. Phys.*, A207, 298
 Pandharipande V. R., 1971, *Nucl. Phys.*, A178, 123
 Sahu P. K., Basu R., Datta B., 1993, *ApJ*, 416, 267
 Stergioulas N., Friedman J. L., 1995, *ApJ*, 444, 306
 Sunyaev R. A., Shakura N. I., 1986, *Sov. Astr. Lett.*, 12, 117
 Walecka J.D., 1974, *Ann. Phys.*, 83, 491
 Wiringa R. B., Fiks V., Fabrocini A., 1988, *Phys. Rev. C*, 38, 1010

This paper has been produced using the Royal Astronomical Society/Blackwell Science \LaTeX style file.

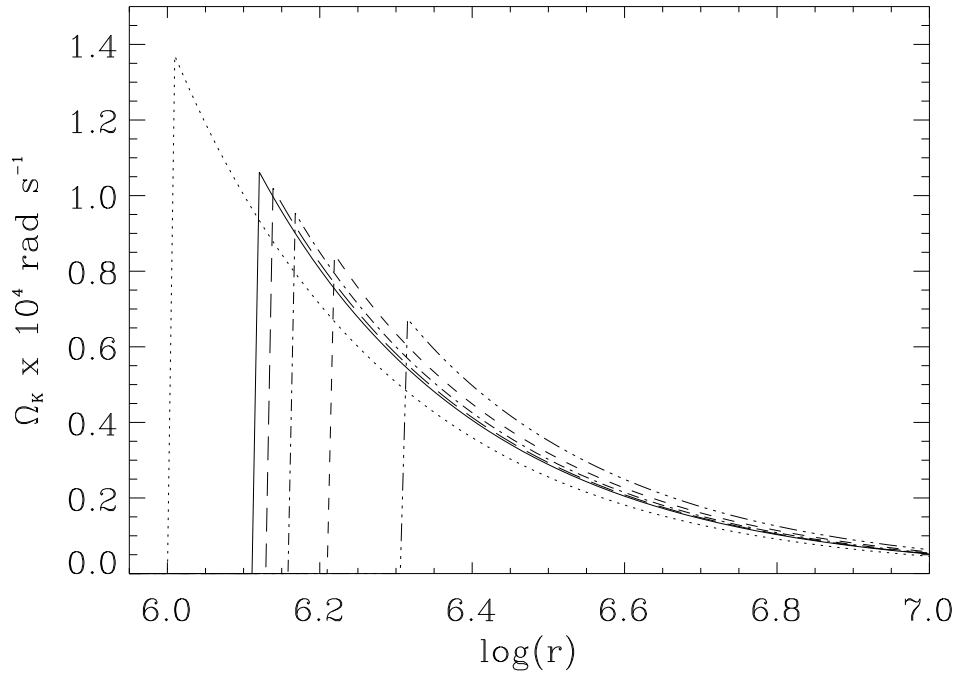


Figure 7. Keplerian angular velocity (Ω_K) profiles for various EOS. The vertical lines indicate the location of the star's surface. The horizontal axis corresponds to the logarithm of the radial coordinate r taken in centimeters.